PHYSICAL REVIEW C VOLUME 16, NUMBER 1 JULY 1977

Optical-model potential in finite nuclei from Reid's hard core interaction

J.-P. Jeukenne, A. Lejeune, and C. Mahaux
Institute of Physics, University of Liège, Sart Tilman, B-4000 Liège 1, Belgium
(Received 17 February 1977)

Starting from the Brueckner-Hartree-Fock approximation and Reid's hard core nucleon-nucleon interaction, we calculate and parametrize the energy—and the density—dependence of the isoscalar, isovector, and Coulomb components of the complex optical-model potential in infinite nuclear matter, for energies up to 160 MeV. We then construct the optical-model potential in a finite nucleus. In a first step, we adopt a local density approximation which implies that the value of the complex potential at each point of the nucleus is the same as in a uniform medium with the local density. We compute the corresponding volume integrals per nucleon and mean square radii of the real and of the imaginary parts of the optical-model potential, in particular for protons scattered by ^{12}C, ^{16}O, ^{27}Al, ^{40}Ca, ^{58}Ni, ^{120}Sn, and ^{208}Pb. We compare these results with a compilation of empirical values and find that the calculated and experimental volume integrals are in good agreement but that the theoretical mean square radii are too small. We ascribe this discrepancy to the fact that our local density approximation does not include accurately the effect in a nonuniform medium of the range of the effective interaction. We include this range in a semiphenomenological way suggested by the Hartree approximation. With a reasonable value for this range parameter, which is the only one occurring in our work, good agreement is obtained between the theoretical and the empirical values of the volume integrals and mean square radii of the real and, to a lesser extent, of the imaginary parts of the optical-model potential, for mass numbers $12 \leq A \leq 208$ and for energies E up to 160 MeV. Our results are given in analytic form and can thus be used in analyses of experimental data. We also discuss the difference between the optical-model potentials for protons and for neutrons.

[NUCLEAR REACTIONS Calculation of the complex optical-model potential for finite nuclei from Reid's hard core interaction; comparison with a compilation of empirical potentials.]

I. INTRODUCTION

The present paper is devoted to the calculation of the complex optical-model potential (OMP) from "next to first" principles, i.e., from a realistic nucleon-nucleon interaction, and to the comparison between these results and a compilation of empirical values. Its aim and limitation are accurately described by Hodgson[1] who emphasized long ago that "nuclear matter theorists should help the optical-model analysts to get some idea of the overall form of the OMP... since one cannot always determine the OMP purely phenomenologically..."; he added that "... also one cannot determine the OMP purely from nuclear matter considerations: What one can do is to use nuclear matter calculations to get some idea of the overall form of the OMP and then use optical-model analyses to make them more precise by comparing with experimental data." Despite these early calls from practitioners of the optical model and the fundamental interest of the problem, progress has been rather slow. We have recently given a critical survey of the main previous theoretical attempts.[2]

It has been argued that the volume integrals of the real[3] and of the imaginary[4,5] parts of the OMP are rather well determined by the scattering data and that, on the average, these quantities vary smoothly with energy and with target mass number. This is further confirmed by the compilation of experimental values that we present in Sec. IV, and which also include the mean square radii. This observation indicates that the main properties of the OMP are characteristic of the nuclear medium and can thus hopefully be evaluated from the investigation of nuclear matter. This is our basic prejudice. We use a theoretical approach which combines Green's function theory and Brueckner's low density expansion for the OMP in nuclear matter.[6] Of course, it must be expected that some finiteness corrections will have to be performed. One of these will be discussed in Sec. VI. Since we are interested here in the properties of the average OMP, we do not include shell effects; we believe that these might, however, be taken into account *a posteriori*.

The present paper is organized as follows. In Sec. II we briefly recall the main theoretical formulas and establish our notation.[7,8] In Sec. III, we parametrize the real and imaginary parts of the OMP in infinite nuclear matter: We include their dependence on incident energy, on density, on the amount of neutron excess, and on the strength of the Coulomb field. We restrict the discussion to the energy domain $0 < E < 160$ MeV,

to the Brueckner-Hartree-Fock approximation, and to Reid's hard core nucleon-nucleon interaction. We have given elsewhere some preliminary results for the intermediate energy range ($E > 150$ MeV)[9] and for corrections to the Brueckner-Hartree-Fock approximation.[7,10] In Sec. V, we construct the OMP in a finite nucleus from a local density approximation which is rather crude but is nevertheless instructive; it introduces no adjustable parameter into the calculation. It consists in assuming that at each point of the nucleus the OMP is the same as in a uniform medium characterized by the local values of the density, of the amount of neutron excess, etc. The comparison with empirical values, previously compiled in Sec. IV, shows that this local density approximation yields good volume integrals but too small mean square radii for the real and for the imaginary parts of the OMP. We argue in Sec. VI that the discrepancy was to be expected since the long-range part of the effective nucleon-nucleon interaction gives rise to surface corrections; the latter are included semiphenomenologically by introducing an adjustable range parameter. With a reasonable value for this single parameter, good agreement is obtained with the empirical values of the volume integrals and mean square radii of the real part and, to a lesser extent, of the imaginary part of the OMP. Section VII is devoted to the discussion of the isovector and Coulomb components of the OMP, to the role of a neutron-rich skin and to the qualitative interpretation of our results. Finally, Sec. VIII contains our conclusions. In the Appendix, we discuss some features of the improved local density approximation of Sec. VI.

II. THEORETICAL FORMULAS

We briefly recall several definitions and formulas which are needed for the calculation of the OMP in nuclear matter in the framework of the Brueckner-Hartree-Fock approximation. Details and justifications can be found in Refs. 7 and 8. We consider successively the isoscalar, the isovector, and the Coulomb components of the OMP.

A. Isoscalar component

The isoscalar component of the OMP is the one which corresponds to symmetric ($N = Z$) and uncharged nuclear matter. Let k_F denote the Fermi momentum and ρ the density:

$$\rho = 2(3\pi^2)^{-1} k_F^{\,3} . \tag{1}$$

The Brueckner reaction matrix $g_\rho[w]$ is related to the nucleon-nucleon potential v by the integral equation

$$g_\rho[w] = v + v \sum_{a,b>k_F} \frac{|\vec{a},\vec{b}\rangle\langle\vec{a},\vec{b}|}{w - e_\rho(a) - e_\rho(b) + i\delta}\, g_\rho[w] , \tag{2}$$

where we have indicated schematically that the sum over $\vec{a}$ and $\vec{b}$ is restricted to plane wave states with momenta $a = |\vec{a}|$, $b = |\vec{b}|$ larger than k_F. In the Brueckner-Hartree-Fock approximation the mass operator is given by

$$M_\rho(k,\mathcal{E}) = \sum_{j<k_F} \langle \vec{j},\vec{k}\,|g_\rho[\,\mathcal{E} + e_\rho(j)]\,|\,\vec{j},\vec{k}\rangle_{\mathfrak{A}} \tag{3}$$

with the following self-consistent choice for the energies $e_\rho(p)$ ($\hbar = 1$):

$$e_\rho(p) = \frac{p^2}{2m} + \mathrm{Re}M_\rho(p, e_\rho(p)) . \tag{4}$$

The symbol $\mathfrak{A}$ in Eq. (3) refers to antisymmetrization. Relation (4) also defines a functional dependence of p on energy and density:

$$E = \frac{p_\rho^{\,2}(E)}{2m} + \mathrm{Re}M_\rho(p_\rho(E), E) . \tag{5}$$

The real and imaginary parts of the isoscalar component of the OMP for a nucleon with energy E are given by

$$V_0(\rho,E) = \mathrm{Re}M_\rho(k_\rho(E), E) , \tag{6}$$

$$W_0(\rho,E) = m[\overline{m}(\rho,E)]^{-1}\, \overline{W}_0(\rho,E) , \tag{7a}$$

$$\overline{W}_0(\rho,E) = \mathrm{Im}M_\rho(k_\rho(E), E) , \tag{7b}$$

where the E mass is defined as follows

$$\overline{m}(\rho,E)/m = \left[1 - \frac{\partial}{\partial\mathcal{E}}\,\mathrm{Re}M_\rho(k_\rho(E),\mathcal{E})\right]_{\mathcal{E}=E} . \tag{8}$$

B. Isovector component

The isovector component of the OMP is the one which arises from neutron excess. Let us denote by ρ_n and ρ_p the neutron and proton densities, respectively. The amount of neutron excess is measured by the asymmetry parameter

$$\alpha = \frac{\rho_n - \rho_p}{\rho_n + \rho_p} = \rho^{-1}(\rho_n - \rho_p) . \tag{9}$$

The corresponding isovector contribution to the OMP is usually written in the form

$$\pm\alpha[V_1(\rho,E) + iW_1(\rho,E)] , \tag{10}$$

where the upper and lower signs refer to neutrons and to protons, respectively. In Ref. 8, we expressed V_1 and W_1 in terms of an auxiliary function $N(E)$ whose Brueckner-Hartree-Fock approximation is given by Eqs. (60b) and (61) of Ref. 8:

$$V_1(\rho,E) = \frac{\tilde{m}(\rho,E)}{m}\,\mathrm{Re}N(\rho,E) , \tag{11}$$

$$W_1(\rho,E) = \frac{m}{\overline{m}(\rho,E)}\,\mathrm{Im}N(\rho,E) , \tag{12}$$

where the k mass $\tilde{m}$ is defined by

$$\frac{\tilde{m}(\rho,E)}{m}=\left[1+mk^{-1}\frac{\partial}{\partial k}\,\mathrm{Re}M_{\rho}(k,E)\right]^{-1}_{k=k_{\rho}(E)}. \quad (13)$$

It is related to the familiar effective mass m^*

$$\frac{m^*(\rho,E)}{m}=1-\frac{d}{dE}\,V_0(\rho,E) \quad (14)$$

by the equation

$$\frac{m^*}{m}=\frac{\tilde{m}}{m}\cdot\frac{\overline{m}}{m}. \quad (15)$$

C. Coulomb component

In first approximation, the role of the Coulomb force which acts on an incident proton amounts to adding the Coulomb field V_C to the OMP. However, the fact that the latter is nonlocal and energy dependent must be taken into account by replacing the energy variable E by $E-V_C$ in all expressions. For instance, the isoscalar component of the OMP for a proton with energy E is given by

$$V_0(\rho,E-V_C)+iW_0(\rho,E-V_C). \quad (16)$$

In order to exhibit the so-called "Coulomb correction," we write expression (16) in the form

$$V_0(\rho,E)+iW_0(\rho,E)+[\Delta_C(\rho,E)+iW_C(\rho,E)], \quad (17)$$

with

$$\Delta_C(\rho,E)=V_0(\rho,E-V_C)-V_0(\rho,E)\simeq\left[\frac{m^*(\rho,E)}{m}-1\right]V_C, \quad (18)$$

$$W_C(\rho,E)=W_0(\rho,E-V_C)-W_0(\rho,E). \quad (19)$$

One has in general[8]

$$\Delta_C(\rho,E)<0, \quad W_C(\rho,E)>0. \quad (20)$$

D. Total optical-model potential

Let us gather the expressions given in Secs. IIA–IIC. The real and imaginary parts of the OMP for a neutron with energy E in uniform nuclear matter with density ρ and neutron excess α read

$$V_n(\rho,E)=V_0(\rho,E)+\alpha V_1(\rho,E), \quad (21)$$

$$W_n(\rho,E)=W_0(\rho,E)+\alpha W_1(\rho,E). \quad (22)$$

In the case of a proton with energy E and in the presence of a Coulomb field V_C, the corresponding quantities are given by

$$V_p(\rho,E)=V_0(\rho,E)+\Delta_C(\rho,E)-\alpha V_1(\rho,E-V_C), \quad (23)$$

$$W_p(\rho,E)=W_0(\rho,E)+W_C(\rho,E)-\alpha W_1(\rho,E-V_C). \quad (24)$$

III. PARAMETRIZATION IN NUCLEAR MATTER

In order to provide the reader with utilizable expressions for the OMP, it is necessary to parametrize our numerical results in analytical form. All the quantities given below are calculated from Reid's hard core nucleon-nucleon potential.[11] We include all the P partial waves but only the S and D partial waves with total angular momentum $J\leq 2$. We consider the energy domain $10<E<160$ MeV. We computed all quantities at about 10 energies in this domain, for the Fermi momenta $k_F=1.4$, 1.35, 1.25, 1.10, 1.00, 0.82, and 0.50 fm^{-1}, respectively.

A. Real part of the optical-model potential

We have parametrized the quantity $V_0(\rho,E)$ in the form

$$V_0(\rho,E)=\sum_{i,j=1}^{3}a_{ij}\rho^iE^{j-1}. \quad (25)$$

The coefficients a_{ij} are gathered in Table I; the units are MeV for V_0 and E and fm^{-3} for ρ. One has, for instance $a_{11}=-974$ MeV fm^3. The choice of the powers of ρ appearing in Eq. (25) is largely arbitrary. The only physical requirement is that for small densities $V_0(\rho,E)$ must become proportional to the probability of having another nucleon in the neighborhood of the incident particle,[12] i.e., to ρ.

The quantity $V_0(\rho,E)$ is intimately related to the potential energy density which plays a central role in the energy density approximation for finite nuclei.[12] We argue in Sec. VI that the ratio V_0/ρ is closely connected with the strength of the effective interaction used in the Thomas-Fermi approximation.[13] In Fig. 1, we plot the ratio $|V_0|/\rho$ versus ρ for the energies 10, 30, 50, 80, and 140 MeV. As expected, this ratio decreases with increasing energy[14,15] and with increasing density.[13] We shall return to these points in Secs. VI and VII.

Expression (25) has been fitted to the calculated values of $V_0(\rho,E)$ in the energy interval $10\leq E\leq 160$ MeV. Hence, it is not very accurate for negative energies; in particular, it should not be used to compute the Fermi energy ϵ_F which is defined by

TABLE I. Coefficients a_{ij} in the expression (25) for $V_0(\rho,E)$.

i \ j	1	2	3
1	-0.9740×10^{3}	0.1126×10^{2}	-0.4250×10^{-1}
2	0.7097×10^{4}	-0.1257×10^{3}	0.5853×10^{0}
3	-0.1953×10^{5}	0.4180×10^{3}	-0.2054×10^{1}

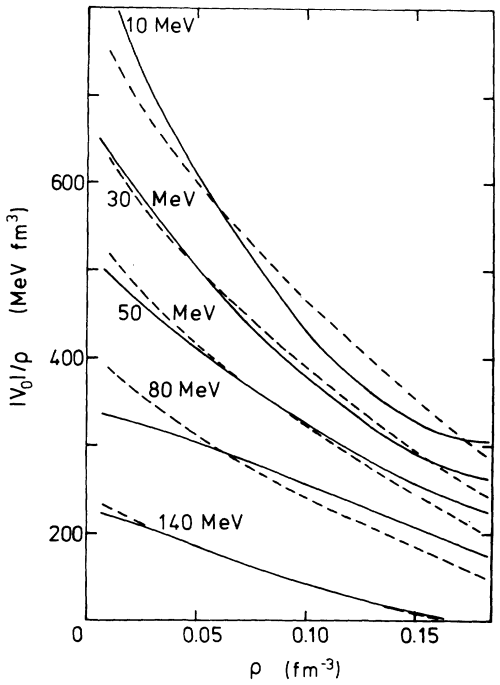

FIG. 1. The full curves represent the dependence on the density of the quantity $|V_0(\rho,E)|/\rho$ for the energies 10, 30, 50, 80, and 140 MeV. The short dashes correspond to the parametrization (A3).

$$\epsilon_F(\rho)=\frac{k_F^2}{2m}+V_0(\rho,\epsilon_F(\rho)). \tag{26}$$

We have calculated ϵ_F from the Brueckner-Hartree-Fock approximation; our result is well reproduced by the expression (ϵ_F in MeV, ρ in fm^{-3})

$$\epsilon_F(\rho)=\rho(-510.8+3222\rho-6250\rho^2). \tag{27}$$

This formula yields $|\epsilon_F|\simeq 26$ MeV at saturation density. This value is larger than the average binding energy per nucleon because it does not include the contribution of the rearrangement potential,[7] which is large at negative energies.

The real part of the quantity N can be parametrized in the form (in MeV)

$$\mathrm{Re}N=\sum_{i,j=1}^{3} b_{ij}\rho^i E^{j-1}. \tag{28}$$

The coefficients b_{ij} are gathered in Table II. Equation (11) shows that the real part of the isovector component of the OMP is obtained by multiplying expression (28) by the k mass. The latter can be fitted as follows:

$$\frac{\tilde{m}(\rho,E)}{m}=1-\sum_{i,j=1}^{3} c_{ij}\rho^i E^{j-1}, \tag{29}$$

TABLE II. Coefficients b_{ij} in the expression (28) for $\mathrm{Re}N_1$.

i \ j	1	2	3
1	0.3601×10^{3}	-0.5224×10^{1}	0.2051×10^{-1}
2	-0.2691×10^{4}	0.5130×10^{2}	-0.2470×10^{0}
3	0.7733×10^{4}	-0.1717×10^{3}	0.8846×10^{0}

with the values shown in Table III. The values of m^* can be calculated from Eqs. (14) and (25) and those of $\bar{m}$ from Eq. (15).

B. Imaginary part of the optical-model potential

The parametric form of the imaginary part of the isoscalar component of the OMP should take into account the fact that it is proportional to $(E-\epsilon_F)^2$ near the Fermi surface. We obtained a good fit to our numerical results with the expression (in MeV)

$$W_0(\rho,E)=\left[1+\frac{D}{(E-\epsilon_F)^2}\right]^{-1}\sum_{i,j=1}^{4} d_{ij}\rho^i E^{j-1}, \tag{30}$$

with $D=600$ MeV^2 and the values of d_{ij} given in Table IV. In Fig. 2, we show the dependence on ρ of the quantity $|W_0(\rho,E)|/\rho$ for the energies 10, 30, 50, 80, and 140 MeV. We note that $|W_0(\rho,E)|$ tends to decrease with increasing energy for $\rho<0.9$ fm^{-3}. At larger densities, the quantity $|W_0(\rho,E)|$ steadily increases with energy. Clearly, these features will yield a transition from surface to volume absorption at about 50 MeV in finite nuclei.

The imaginary part of N [see Eq. (12)] behaves like $(E-\epsilon_F)$ near the Fermi surface.[16] Therefore, we parametrized it in the form (in MeV)

$$\mathrm{Im}N_1(\rho,E)=\left[1+\frac{F}{E-\epsilon_F}\right]^{-1}\sum_{i,j=1}^{4} f_{ij}\rho^i E^{j-1}. \tag{31}$$

It turns out that the value of F determined from the fit in the energy interval $10\leq E\leq 160$ MeV is so small that the first factor on the right-hand side of Eq. (31) is of aesthetical rather than practical value. We took $F=1$ MeV. The other coefficients are listed in Table V.

TABLE III. Coefficients c_{ij} in the expression (29) for $\tilde{m}(\rho,E)$.

i \ j	1	2	3
1	0.4557×10^{1}	-0.5291×10^{-2}	0.6108×10^{-5}
2	-0.2051×10^{1}	-0.4906×10^{0}	0.1812×10^{-2}
3	-0.6509×10^{2}	0.3095×10^{1}	-0.1190×10^{-1}

TABLE IV. Coefficients d_{ij} in the expression (30) for $W_0(\rho, E)$.

i \ j	1	2	3	4
1	-0.1483×10^{4}	0.3718×10^{2}	-0.3549×10^{0}	0.1119×10^{-2}
2	0.2988×10^{5}	-0.9318×10^{3}	0.9591×10^{1}	-0.3160×10^{-1}
3	-0.2128×10^{6}	0.7209×10^{4}	-0.7752×10^{2}	0.2611×10^{0}
4	0.5125×10^{6}	-0.1796×10^{5}	0.1980×10^{3}	-0.6753×10^{0}

IV. COMPILATION OF EMPIRICAL VALUES

We shall mainly discuss the OMP for protons; the difference between the OMP for neutrons and for protons will be considered in Sec. VII. It has been repeatedly observed[3,17] that the differential and total cross sections generated from various OMP are rather insensitive to the detailed form of the latter provided that the various OMP have the same volume integral per nucleon

$$J_V/A = -A^{-1}\int V(r)d^3r \tag{32}$$

and the same root mean square radius

$$\langle R_V^2\rangle^{1/2} = \left[\frac{\int V(r)r^2 d^3r}{\int V(r)d^3r}\right]^{1/2}. \tag{33}$$

Recently, it has been shown that an analogous property also holds, although less strictly, for the volume integral per nucleon of the imaginary part of the OMP[4,5]:

$$J_W/A = -A^{-1}\int W(r)d^3r\,; \tag{34}$$

it has also been claimed[17] to be valid for the root mean square radius of the imaginary part

$$\langle R_W^2\rangle^{1/2} = \left[\frac{\int W(r)r^2 d^3r}{\int W(r)d^3r}\right]^{1/2}. \tag{35}$$

All these features will be confirmed and exhibited below. Thus, a meaningful test for the agreement between a calculated and an empirical OMP consists in comparing their volume integrals and root mean square radii.

We have calculated the values of J_V/A, $\langle R_V^2\rangle$, J_W/A, and $\langle R_W^2\rangle$ for the empirical OMP compiled by Perey and Perey[18] for the nuclei ^{12}C, ^{16}O, ^{27}Al, ^{40}Ca, ^{58}Ni, ^{120}Sn, and ^{208}Pb. Whenever possible, we only retained those phenomenological OMP which yield fits considered as "good" or "very good" by Perey and Perey; the corresponding values are represented by full dots in Figs. 3–16, where the open dots correspond to "acceptable" fits which were used when no better choice was available. Whenever several phenomenological OMP existed in a narrow energy domain, we have averaged them over a 5 MeV interval, in order to simplify the figures. Then, the dot represents the average value, while the error bar shows the standard error (standard deviation of the mean value).

The fact that the empirical values plotted in Figs. 3–16 show only little dispersion about a smooth function of energy confirms that the scattering data determine fairly well the lowest moments (32)–(35) of the OMP. On the average, the quantity J_V/A decreases practically linearly with increasing energy for $10 \leq E \leq 70$ MeV; the decreasing rate becomes smaller for larger energies. The mean square radius $\langle R_V^2\rangle$ is essentially independent of energy; this also holds true for $\langle R_W^2\rangle$, but in the latter case the empirical values show more dispersion. In general, it appears that J_W/A tends to increase with energy for $E < 20$ MeV. The A dependence of these quantities will be discussed in Sec. VII.

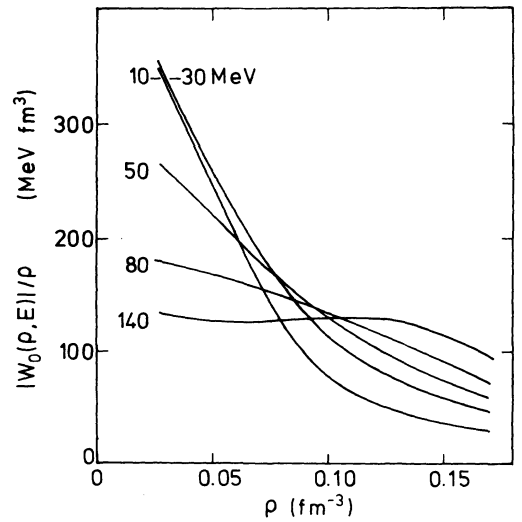

FIG. 2. Dependence on the density ρ of the quantity $|W_0(\rho, E)|/\rho$, where W_0 is the isoscalar component of the OMP, for the energies 10, 30, 50, 80, and 140 MeV.

V. LOCAL DENSITY APPROXIMATION

A. Definition

In the present section, we construct the OMP in a finite nucleus from the assumption that at a dis-

TABLE V. Coefficients f_{ij} in the expression (31) for $\mathrm{Im}N_1$.

i \ j	1	2	3	4
1	0.5461×10^{3}	-0.1120×10^{2}	0.1065×10^{0}	-0.3541×10^{-3}
2	-0.8471×10^{4}	0.2300×10^{3}	-0.2439×10^{1}	0.8544×10^{-2}
3	0.5172×10^{5}	-0.1520×10^{4}	0.1717×10^{2}	-0.6211×10^{-1}
4	-0.1140×10^{6}	0.3543×10^{4}	-0.4169×10^{2}	0.1537×10^{0}

tance r from the nuclear center, where the density is equal to $\rho(r)$, the OMP is given by [see Eqs. (21)–(24)]

$$V_E(r)+iW_E(r)=V(\rho(r),E)+iW(\rho(r),E). \tag{36}$$

In other words, this local density approximation (LDA) ascribes to the OMP at the density $\rho(r)$ the same value as in a uniform medium with the same value of the density, with the same neutron excess, and at the same energy. This LDA is rather crude, but the comparison of its predictions with experiment will be instructive. It will be improved upon in Sec. VI.

The input of our calculation consists in two ingredients, namely, the nuclear matter results presented in Sec. III on the one hand and density distributions for protons and neutrons on the other hand. Except in Sec. VII D, we assume for simplicity that the density distributions of the protons and of the neutrons have the same geometry and are given by the following average expression, proposed by Negele[19]

$$\rho^{(\kappa)}(r)=\frac{\rho_0^{(\kappa)}}{1+\exp[(r-C_\rho)/a_\rho]}, \tag{37}$$

where

$$a_\rho=0.54\ \mathrm{fm}, \qquad C_\rho=(0.978+0.0206A^{1/3})A^{1/3}\ \mathrm{fm}, \tag{38}$$

$$\rho_0^{(\kappa)}=\frac{3\kappa}{4\pi C_\rho^{3}(1+\pi^2a_\rho^{2}/C_\rho^{2})}, \quad \kappa=N \text{ or } Z. \tag{39}$$

This parametrization reproduces reasonably well the experimental charge density distribution; its accuracy is poorer for light nuclei or in the extreme tail. It is appropriate to utilize here such an "average" expression for the density since we deal with the "global" OMP rather than with a specific nucleus.

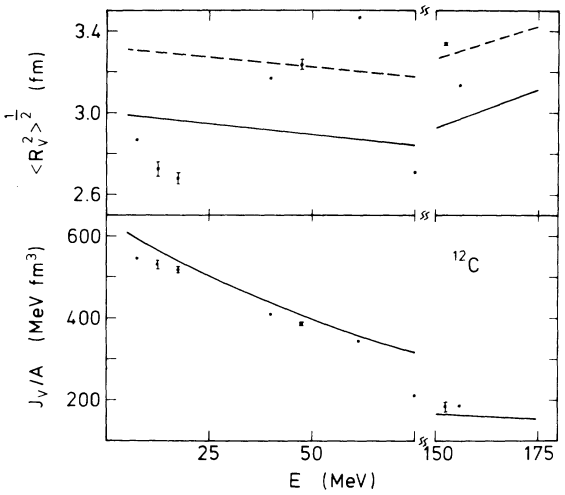

FIG. 3. The dots in the upper and lower parts represent the empirical values of the root mean square radius and of the volume integral per nucleon of the real part of the proton OMP of ^{12}C. The compilation of Perey and Perey (Ref. 18) has been used. The full dots correspond to "good" or "very good" fits; the open dots to "acceptable" or poorer fits. The full curves show the theoretical result of the LDA (Sec. V). The long dashes correspond to the improved LDA of Sec. VI, with a range $t=1.2$ fm.

B. Real part of the OMP

The full curves in Figs. 3–9 show the dependence on energy of the quantities J_V/A and $\langle R_V^2\rangle^{1/2}$, as calculated from the LDA in the case of protons. The agreement between theoretical and empirical values of J_V/A is excellent in the whole energy range $0<E<170$ MeV. This agreement is much

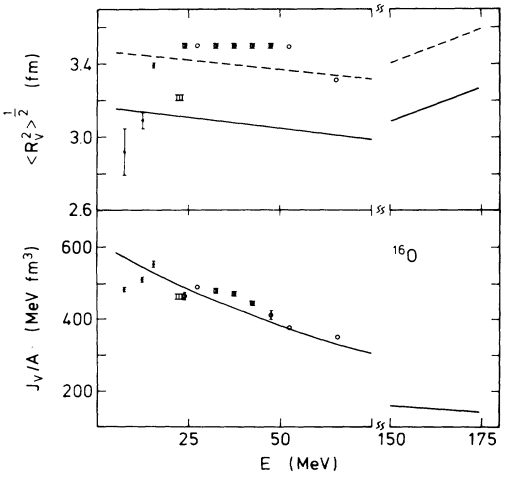

FIG. 4. Same as Fig. 3, for ^{16}O. The open squares at $E=22.5$ MeV are obtained from Ref. 37.

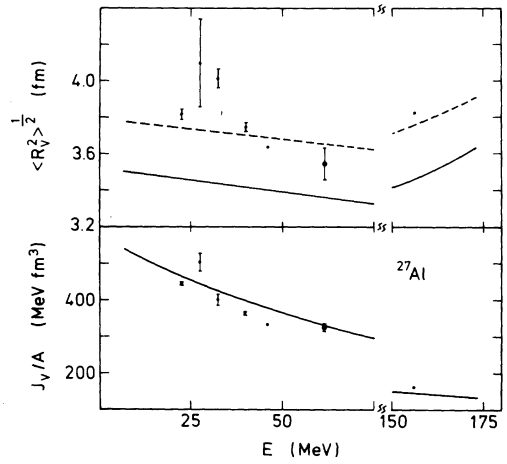

FIG. 5. Same as Fig. 3, for ^{27}Al.

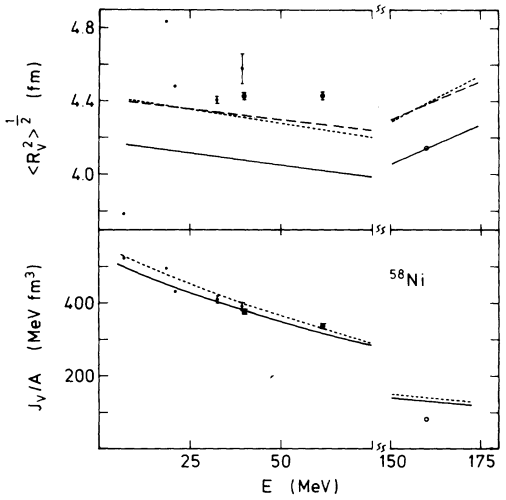

FIG. 7. Same as Fig. 3, for ^{58}Ni. The short dashes correspond to the Eq. (A1), with $b = 1$ fm.

better than that attained in previous theoretical approaches.[2] However, the calculated values of $\langle R_V^2 \rangle^{1/2}$ are systematically too small, thus indicating that the surface of the potential well is not well reproduced. The calculated potential well has a Woods-Saxon shape. In the example of ^{208}Pb at $E = 30$ MeV, its depth, half-depth radius, and diffuseness are equal to

$$U_V = -56 \text{ MeV}, \quad C_V = 1.19A^{1/3} \text{ fm}, \quad a_V = 0.53 \text{ fm}. \tag{40}$$

The calculated diffuseness is thus significantly smaller than that used in empirical analyses ($a_V \simeq 0.65$ fm). This turns out to be the case for all nuclei and is probably the main origin of the too small root mean square radii that we obtain from the LDA. We note, however, that Dover and Van Giai[20] find good agreement between the empirical mean square radii and those computed from a density-dependent Hartree-Fock approximation with a Skyrme interaction, although their calculated diffuseness is also too small ($a = 0.52$ fm).

C. Imaginary part of the OMP

Figures 10–16 show that the calculated values of J_W/A are usually slightly larger than the empirical values. However, one should keep in mind that all the nuclei considered here are singly or doubly magic. It has been suggested by several authors that the imaginary part of the OMP for such nuclei is smaller than on the average, because the density

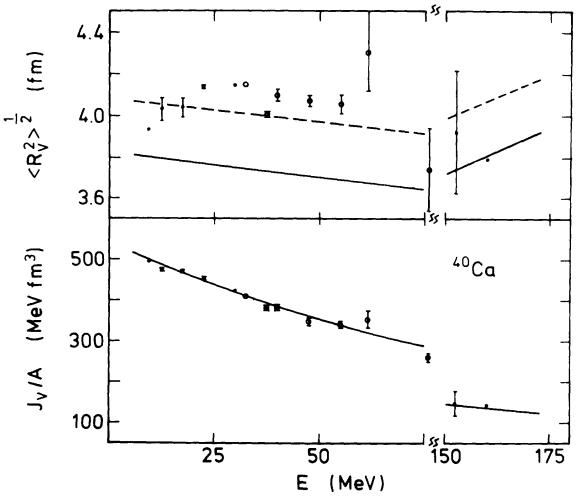

FIG. 6. Same as Fig. 3, for ^{40}Ca.

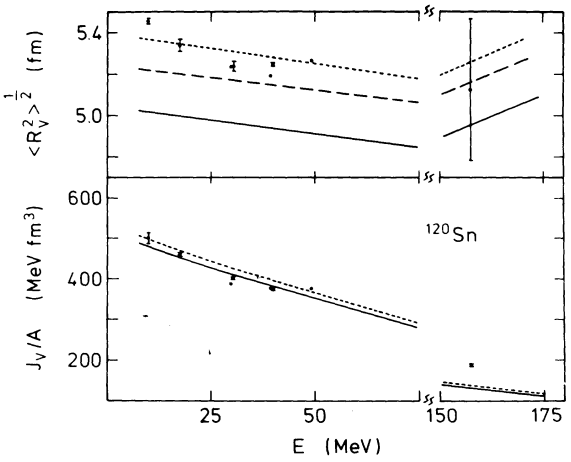

FIG. 8. Same as Fig. 3, for ^{120}Sn. The short dashes correspond to the assumption that a neutron-rich skin exists (Sec. VII D).

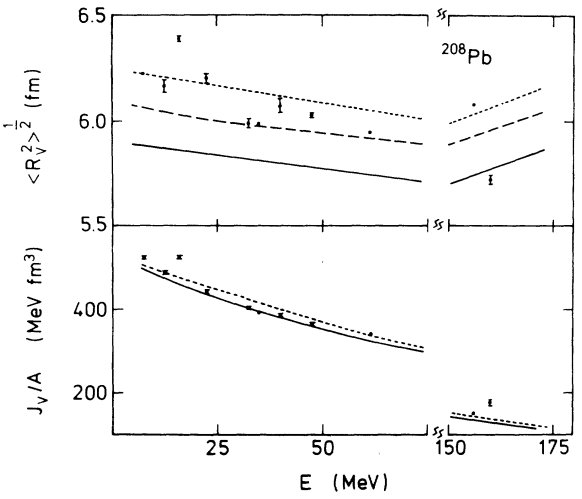

FIG. 9. Same as Fig. 3, for ^{208}Pb. The short dashes correspond to a neutron-rich skin (Sec. VII D).

of compound nuclear states is smaller and the inelastic channel thresholds lie higher. We return to this point below.

The energy dependence of J_W/A is well reproduced, for instance in the case of ^{208}Pb where numerous accurate empirical values are available. The rapid increase of the OMP with energy for $E<20$ MeV is mainly due to the imaginary part W_C of the Coulomb correction [Eq. (19)]. This is apparent from Fig. 16, where the dash-and-dot line represents the negative of the quantity

$$J_{W_C}/A = -A^{-1} \int W_C(r) d^3r . \tag{41}$$

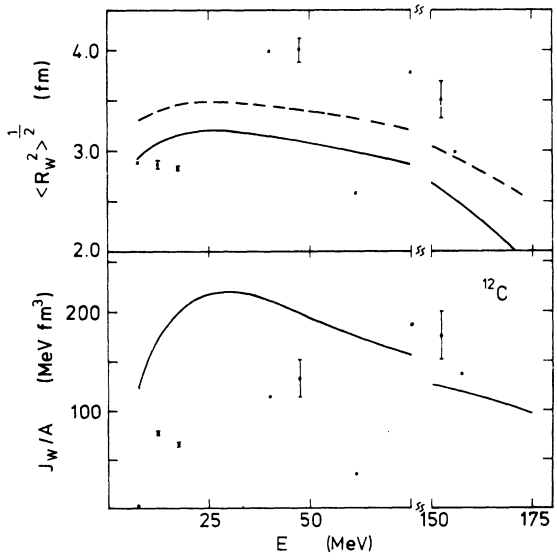

FIG. 10. Same as Fig. 3, for the imaginary part of the OMP.

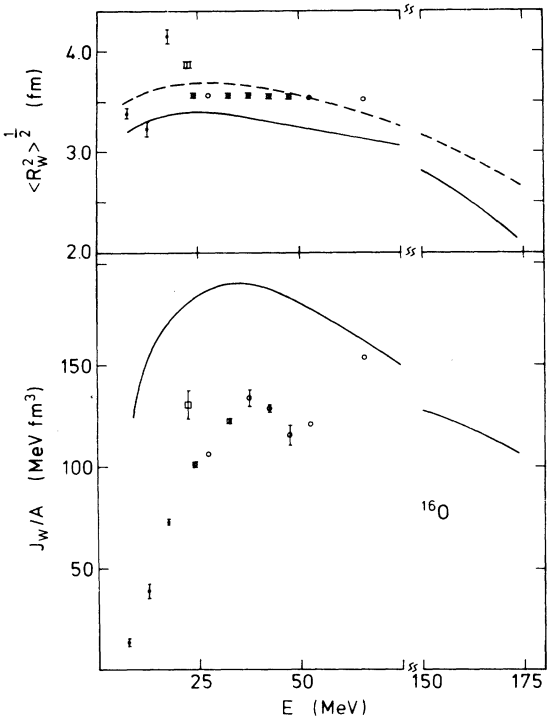

FIG. 11. Same as Fig. 4, for the imaginary part of the OMP.

This imaginary Coulomb correction is responsible for the difference between the curve shown in Fig. 16, where W_C is included, and the preliminary results given in Ref. 5, where the contribution of W_C was omitted. It must be stated, however, that our LDA is not accurate below the Coulomb barrier. This shows up dramatically in the fact that

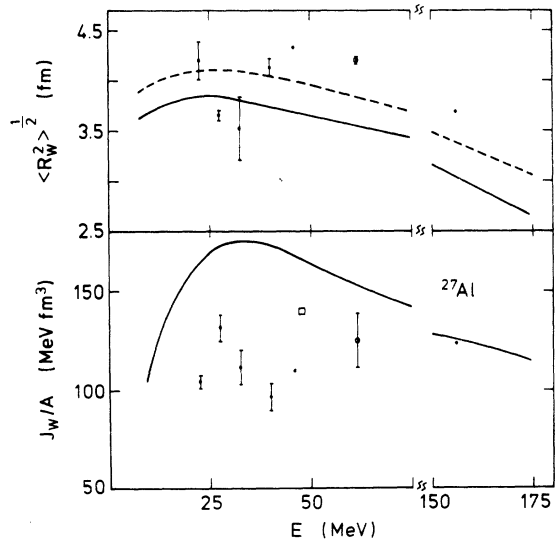

FIG. 12. Same as Fig. 5, for the imaginary part of the OMP.

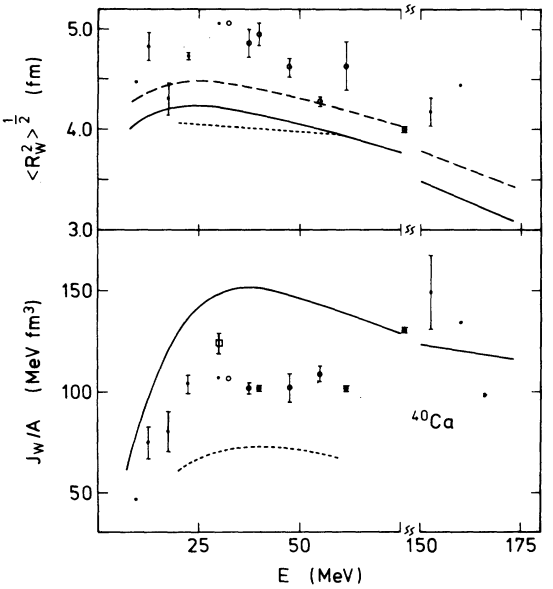

FIG. 13. Same as Fig. 6, for the imaginary part of the OMP. The short dashes are calculated from the theoretical results of Vinh Mau and Bouyssy (Ref. 21).

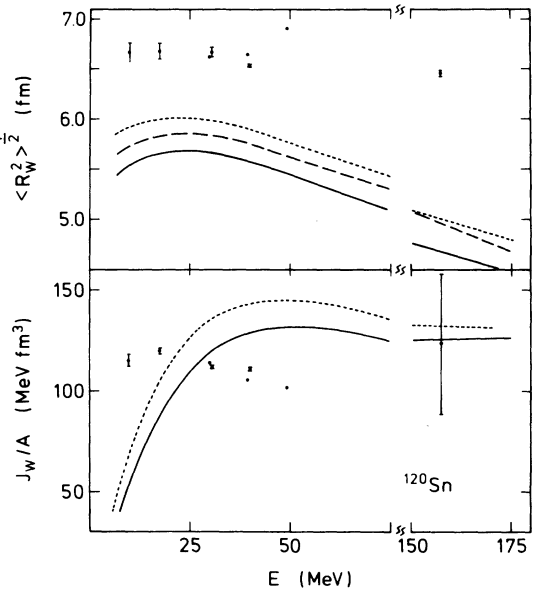

FIG. 15. Same as Fig. 8, for the imaginary part of the OMP. The short dashes correspond to a neutron-rich skin (Sec VII D).

the value of $\epsilon_F^{(p)} = \epsilon_F + V_C$, which is the Fermi energy of the protons in the LDA, is positive in the surface region in the case of ^{208}Pb. According to the parametrization (30), the value of $W_0(E - V_C) = W_0(E) + W_C$ vanishes for $E < \epsilon_F^{(p)}$. This difficulty is related to the fact that the LDA is a quasiclassical approximation which is thus questionable in the classically forbidden regions. However, this difficulty is encountered only at low energy, for instance at $E < 10$ MeV in the most unfavorable

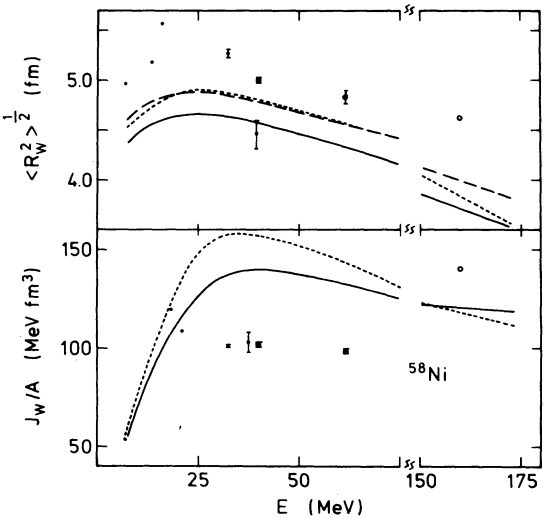

FIG. 14. Same as Fig. 7, for the imaginary part of the OMP.

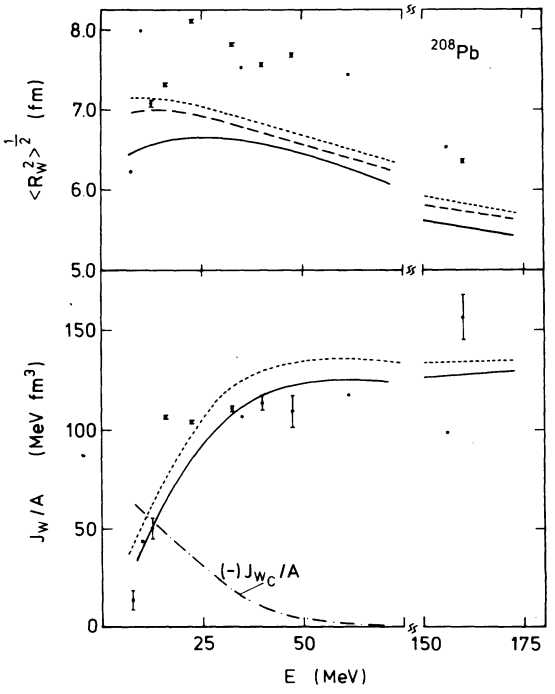

FIG. 16. Same as Fig. 9, for the imaginary part of the OMP. The dash-and-dots represent the Coulomb correction J_{W_C}/A. The short dashes correspond to a neutron-rich skin (Sec. VII D).

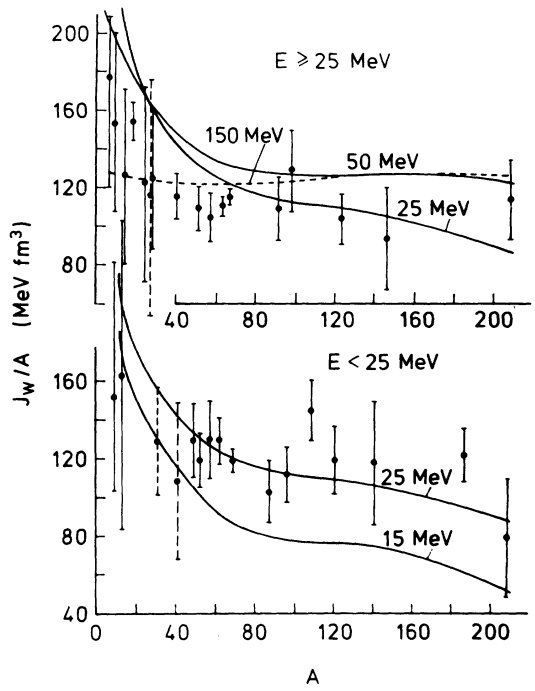

FIG. 17. The dots and error bars represent the dependence on mass number of the empirical values of the volume integral per nucleon of the imaginary part of the OMP, as compiled by Hodgson (Ref. 5), for proton energies $E \geq 25$ MeV (upper part) and $E < 25$ MeV, respectively. The full curves show the theoretical results derived from the LDA at $E = 15$, 25, and 50 MeV. The short dashes correspond to $E = 150$ MeV.

case of ^{208}Pb, and in a narrow range of values for the radial distance r.

The dotted curve in Fig. 13 represents the values of J_W/A and of $\langle R_W^2\rangle^{1/2}$ that we computed from Figs. 22–25 of the recent paper by Vinh Mau and Bouyssy.[21] These authors performed a microscopic calculation of $W(r)$ in ^{40}Ca; they used a random phase approximation for the OMP, together with a phenomenological nucleon-nucleon interaction fitted to the properties of low-lying bound states. We see that their computed volume integral is somewhat too small, while ours is too large; their root mean square radius is about the same as ours.

In order to smooth out the shell effects, it is of interest to consider the dependence on energy or on mass number of J_W/A when the latter quantity is averaged over mass numbers or over energy, respectively. In Fig. 17, we show the dependence on A of empirical values of J_W/A averaged over energy in the two energy domains $E < 25$ MeV and $E \geq 25$ MeV.[5] The full dots and standard deviations are taken from the recent compilation by Hodgson.[5] We have, however, left out from the latter the value corresponding to $A = 16$, since it appears to include an error due to the use of the derivative of a Woods-Saxon instead of a Gaussian, for the form factor of the surface absorption given in Ref. 22. The same error affects some of the empirical values of J_W/A for ^{27}Al and ^{40}Ca; the corresponding error bars are represented by dashed lines in Fig. 17. The full curves show the results of our LDA for $E = 20$, 25, and 50 MeV. We see that the average behavior of the empirical values is quite well reproduced, in particular the rise of J_W/A with decreasing mass number. We discuss this trend in Sec. VII C.

Finally, the full curves in the upper parts of Figs. 10–16 show the energy dependence of the LDA values of $\langle R_W^2\rangle^{1/2}$. We see that the calculated root mean square radii are significantly smaller than the empirical ones. This discrepancy is even larger than in the case of $\langle R_V^2\rangle^{1/2}$. As in the latter case, it reflects the fact that the calculated radial form factor is too steep at the nuclear surface. For instance, the function $W(r)$ in the case of ^{208}Pb at 30 MeV can be fitted by the expression

$$W(r) = W_V f_W(r) - 4W_S a_W \frac{d}{dr} f_W(r) , \tag{42}$$

$$f_W(r) = \left(1 + \exp\frac{r - R_W}{a_W}\right)^{-1} , \tag{43}$$

with the numerical values

$$W_V = -5.0 \text{ MeV} , \quad W_S = -12.7 \text{ MeV} ,$$

$$R_W = 1.14A^{1/3} \text{ fm} , \quad a_W = 0.52 \text{ fm} .$$

The diffuseness a_W is significantly smaller than the value $a_W \approx 0.7$ fm which is usually adopted in empirical analyses.

VI. IMPROVED LOCAL DENSITY APPROXIMATION

A. Weakness of the LDA

The LDA yields good agreement between the theoretical and the empirical values of the volume integrals per nucleon of the real and of the imaginary parts of the OMP. This indicates that the Brueckner-Hartree-Fock and local density approximations are fairly satisfactory in the central region of the nucleus. However, the calculated root mean square radii are systematically too small. This suggests that the LDA is not accurate in the surface region. This is not surprising since improved approximations based on nuclear matter results usually involve surface corrections, sometimes expressed in terms of derivatives of the local density as in the Thomas-Fermi[13] and energy-density[12] approaches.

In order to exhibit the main weakness of the LDA which has been adopted in Sec. V, we consider the

following simple model. We assume that the nucleon-nucleon interaction $v(r)$ only depends on the relative distance r between the two nucleons and is sufficiently weak to justify the use of first order perturbation theory. Let us furthermore only retain the direct (Hartree) contribution to the (real) OMP and omit the exchange (Fock) term. In a finite nucleus, the Hartree approximation reads

$$V^{\mathrm{FN}}(r) = C \int d^3r' v(|\vec{r} - \vec{r}'|)\rho(r') , \tag{44}$$

where C is a spin-statistical factor. In nuclear matter with density ρ, the Hartree potential is given by

$$V^{\mathrm{NM}} = C\rho \int d^3r' v(r') ; \tag{45}$$

if the LDA of Sec. V is used, the resulting expression for the OMP reads

$$V^{\mathrm{LDA}}(r) = C\rho(r) \int d^3r' v(r') . \tag{46}$$

It is only in the case of a zero-range interaction that the LDA (46) becomes identical to the more correct expression (44): because of the finite range of the interaction, approximations (44) and (46) thus differ in a nonuniform medium. We note that this discussion remains qualitatively valid for a density-dependent interaction.

Sometimes, the difference between (44) and (46) is expressed in terms of derivatives of the local density. This is suggested by the expansion[12]

$$V^{\mathrm{FN}}(r) = V^{\mathrm{LDA}}(r) + \tfrac{1}{6} v_2 \Delta\rho + \tfrac{1}{120} v_4 \Delta^2\rho , \tag{47}$$

where

$$v_n = C \int d^3r' r'^n v(r') . \tag{48}$$

In practice, the domain of validity of the expansion (47) is quite limited, and the coefficients of the gradient terms are thus treated as phenomenological parameters in the energy-density formalism.[12]

Another possible approach consists in retaining the effect of the range of the effective interaction in the calculation of the mean potential field, as for instance in the Thomas-Fermi approximation.[23] It is the latter point of view that we adopt below.

B. Improved local density approximation

Equation (45) suggests to identify the strength of the effective interaction with the energy- and density-dependent quantity

$$v_E(\rho) = \frac{V(\rho, E)}{\rho} , \tag{49}$$

where V is the real part of the OMP [Eqs. (21) and (23)]. The contribution to this quantity of the isoscalar component of the OMP has been plotted versus density in Fig. 1, which is discussed further in the Appendix. We now introduce a range for the interaction (49). For simplicity, we adopt a Gaussian form factor:

$$v_E(\rho, |\vec{r} - \vec{r}'|) = (t\sqrt{\pi})^{-3} \exp(-|\vec{r} - \vec{r}'|^2/t^2) v_E(\rho) . \tag{50}$$

In view of the fact that the justification of our procedure is only qualitative, we did not consider other expressions for the form factor.

Equations (44) and (50) lead to the following "improved" LDA for the real part of the OMP:

$$\tilde{V}_E(r) = (t\sqrt{\pi})^{-3} \int v_E(\rho(r')) \times \exp(-|r - r'|^2/t^2)\rho(r') d^3r' \tag{51a}$$

$$= (t\sqrt{\pi})^{-3} \int V_E(r') \exp(-|\vec{r} - \vec{r}'|^2/t^2) d^3r' , \tag{51b}$$

where $V_E(r')$ is the LDA value defined in Eq. (36). The normalization factor on the right-hand side of Eq. (50) was chosen in such a way that $\tilde{V}_E(r) = V_E(r)$ in a uniform medium, as should be the case according to our discussion in Sec. VI A. We note that the use of $\rho(r')$ instead of $\rho(r)$ as argument of v_E in Eq. (51a) is arbitrary. The difference between these two choices should be negligible for a sufficiently small value of the range t, and is discussed further in the Appendix. Here, we adopt the choice (51a) because it facilitates the theoretical interpretation of our numerical results.

From the multiple scattering approach, we expect that finite range corrections to the LDA must also be introduced for the imaginary part in the surface region. Therefore, it may be instructive to show numerical results for the quantity

$$\tilde{W}_E(r) = (t\sqrt{\pi})^{-3} \int W_E(r') \exp(-|\vec{r} - \vec{r}'|^2/t^2) d^3r' , \tag{52}$$

although the theoretical foundation of this folding formula is more shaky than that of Eq. (51a). In particular, it is likely that the range t in Eq. (52) should be larger than in Eq. (51a) because it is mainly the long-range part of the effective nucleon-nucleon interaction which is responsible for the imaginary part of the OMP.

C. Numerical results

The main geometrical differences between the improved LDA $\tilde{V}_E(r)$ and the LDA $V_E(r)$ can be figured out from the work of Süssmann[24] and of Myers[25] on leptodermous distributions. Let us,

for definiteness, consider the case where $V(r)$ has the Woods-Saxon shape

$$V(r)=\frac{U}{1+\exp(r-C_V/a_V)}\,,\quad C_V=r_V A^{1/3}. \tag{53}$$

In the limit

$$\frac{t}{C_V}\ll 1\,,\quad \frac{a_V}{C_V}\ll 1\,, \tag{54}$$

the folded potential $\tilde{V}_E(r)$ also has a Woods-Saxon shape, with the following values of the depth, half-depth radius, diffuseness,[25]

$$\tilde{U}=U\,,\quad \tilde{C}_V=C_V\left(1-\frac{1}{2}\,\frac{t^2}{C_V^2}\right), \tag{55}$$

$$\tilde{a}_V=\left(a_V^2+\frac{3}{2\pi^2}\,t^2\right)^{1/2}. \tag{56}$$

In the limit (54), the volume integrals of $\tilde{V}(r)$ and $V(r)$ are equal

$$J_{\tilde{V}}/A=J_V/A\,, \tag{57}$$

but the root mean square radii differ

$$\langle R_{\tilde{V}}^2\rangle^{1/2}=\langle R_V^2\rangle^{1/2}\left(1+\frac{5}{4}\,\frac{t^2}{C_V^2}\right). \tag{58}$$

Relation (57) indicates that the good agreement obtained in Sec. V between the empirical and calculated volume integrals per nucleon will not be spoiled in the improved LDA. Equation (58) shows that the inclusion of the finite range effects will lead to an improvement of the comparison between empirical and calculated root mean square radii. The long dashes in Figs. 3–9 show the dependence on energy of the root mean square radius $\langle R_{\tilde{V}}^2\rangle^{1/2}$, in the case

$$t=1.2\text{ fm}. \tag{59}$$

As expected from Eq. (57), the volume integral per nucleon $J_{\tilde{V}}/A$ is so close to J_V/A that these two quantities cannot be distinguished graphically.

We show the energy dependence of the quantities $J_{\tilde{W}}/A$ and $\langle R_{\tilde{W}}^2\rangle^{1/2}$ in Figs. 10–16, for $t=1.2$ fm. In most cases, the values of $J_{\tilde{W}}/A$ and of J_W/A cannot be distinguished graphically. The introduction of a range t appears to reduce somewhat the discrepancy between theoretical and calculated root mean square radii for the imaginary part of the OMP, without eliminating it for heavy nuclei.

In view of the semiphenomenological nature of our improved LDA, no intimate relationship exists between the numerical value (59) for the range parameter t and the actual range of "the" effective interaction. We return to this point in the Appendix. We note, however, that the value $t=1.2$ fm is close to the range of commonly used phenomenological effective interactions (see, e.g., Ref. 26).

The real part of the folded potential well can be fitted with a Woods-Saxon formula. In the case of ^{208}Pb at 30 MeV, the corresponding parameters are

$$\tilde{U}_p=-53.6\text{ MeV}\,,\quad \tilde{C}_V=1.21A^{1/3}\,,\quad \tilde{a}_V=0.62\text{ fm}\,, \tag{60}$$

which should be compared with the values given in Eq. (40). The imaginary part of the folded potential can be fitted by expression (41). In the case of ^{208}Pb at $E=30$ MeV, the parameters (43) become

$$\tilde{W}_V=-5.8\text{ MeV}\,,\quad \tilde{W}_S=-7.9\text{ MeV}\,,$$
$$\tilde{R}_W=1.19A^{1/3}\text{ fm}\,,\quad \tilde{a}_W=0.61\text{ fm}\,. \tag{61}$$

D. Discussion

The validity of the LDA at low energy, in its simplest or improved form, has often been questioned (see Ref. 27, and references contained therein). We indicated in Sec. VI that our theory truly aims at calculating the strength of the effective interaction. In a more sophisticated version (cf. Appendix), it could be used to find not only the strength, but also the form factor of this interaction. Hence, the LDA corresponds to the construction of the density-dependent effective interaction V_0/ρ, in the spirit of density dependent Hartree-Fock calculations. In its improved form (i.e., with due account of finite range effects), it requires that the strength of the effective interaction varies only little over the range of the interaction, i.e., that

$$\left|t\,\frac{d\rho}{dr}\,\frac{d}{d\rho}\left(\frac{V_0}{\rho}\right)\right|\ll\left|\frac{V_0}{\rho}\right|\,. \tag{62}$$

In the Appendix, we show that the following formula[25] is a fair approximation:

$$\frac{V_0}{\rho}\approx F(E)(1-d\rho^{2/3})\,, \tag{63}$$

where $d\approx 2$ fm^2 and $F(E)$ is density independent. Evaluating the left-hand side of (62) at $r=R_\rho$, where $|d\rho/dr|$ is largest, one finds the condition

$$t\ll 2.4\text{ fm}\,, \tag{64}$$

which is reasonably well fulfilled. Of course, one should keep in mind that our LDA involves a number of approximations besides inequality (62), for instance the use of the Brueckner-Hartree-Fock approximation and the neglect of shell effects.

VII. DIFFERENCE BETWEEN PROTON AND NEUTRON POTENTIALS

A. Dependence of J_V/A on mass number

Equations (21)–(24) show that the origin of the difference between the OMP for neutrons and protons lies in the Coulomb correction $\Delta_C + iW_C$ on the one hand, and in the symmetry (isovector) potential on the other hand.

In Fig. 18, we represent the dependence on A of the following quantities, at $E = 35$ MeV:

$$J_{V_p}/A = -A^{-1}\int V_p(r,E)d^3r\,, \tag{65}$$

$$J_{\Delta_C}/A = -A^{-1}\int \Delta_C(r,E)d^3r\,, \tag{66}$$

$$J_{V_1}/A = -\alpha A^{-1}\int V_1(r,E)d^3r\,. \tag{67}$$

The full curves are drawn through values calculated in the framework of the LDA for the nuclei ^{12}C, ^{16}O, ^{27}Al, ^{40}Ca, ^{58}Ni, ^{120}Sn, ^{169}Tm, and ^{208}Pb, whence the vanishing of J_{V_1}/A for $A = 12$, 16, and 40 ($\alpha = 0$). The long dashes correspond to the empirical proton potentials of Ref. 28 ($A > 40$). While the calculated and empirical values of the volume integral of the full potential are in very good agreement, Fig. 18 shows that the calculated Coulomb correction is larger than was assumed in Ref. 28.

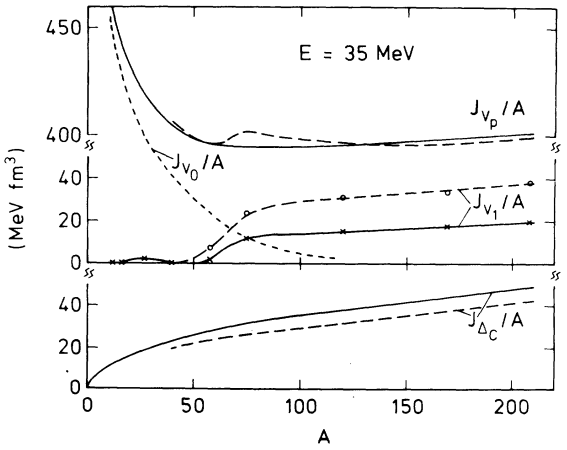

FIG. 18. The full curves represent the A dependence of the volume integrals per nucleon of the real part of the proton OMP, of the Coulomb correction, and of the isovector component [Eqs. (65)–(67)], at $E = 35$ MeV. The long dashes correspond to the empirical proton OMP of Ref. 28. These curves are drawn through the values calculated for the nuclei ^{12}C, ^{16}O, ^{27}Al, ^{40}Ca, ^{58}Ni, ^{120}Sn, ^{169}Tm, and ^{208}Pb, and indicated by open circles and by crosses on the curves marked J_{V_1}/A. The short dashes represent the contribution J_{V_0}/A of the isoscalar component.

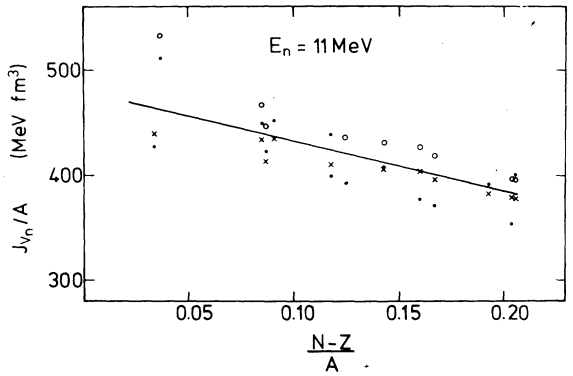

FIG. 19. The crosses represent our calculated values of the volume integral of the real part of the OMP for neutrons (Sec. VI) for $E_n = 11$ MeV, the open circles and the full dots show the empirical values given in Ref. 32. The full straight line is a least square fit to the empirical values of Ref. 31, for $E_n = 8$ MeV.

We discussed the origin of this finding in Ref. 8: It is related to the fact that the geometrical characteristics of V_0 and of Δ_C are different. In the case of ^{40}Ca, the ratio of our calculated Coulomb correction to the standard one is equal to 1.2, in excellent agreement with the value 0.48/0.40 = 1.2 recently deduced by Rapaport *et al.*[29] from the comparison between proton and neutron scattering data.

In Fig. 19, we compare our theoretical results (crosses) of the volume integral per nucleon in the case of neutrons with the empirical values of Holmqvist and Wiedling[30,31] (full curve) and of Ferrer, Carlson, and Rapaport[32]; in their analysis of the data, the latter authors used either an average geometry (open circles) or a geometry which is allowed to change from nucleus to nucleus (full circles). We see that the agreement between theoretical and empirical values is good, despite the fact that in the nuclear interior our calculated value for the isovector component (V_1) of the OMP is smaller than the one which is usually quoted. This confirms the conclusions of Ref. 8.

B. Discussion

In the present section, we give a qualitative explanation for the dependence on mass number of the volume integral per nucleon of the real part of the OMP. Figure 18 shows that the volume integral per nucleon of the isoscalar component of the OMP decreases monotonously with increasing mass number, and that this decrease is steeper for $A < 50$. For $E = 35$ MeV for instance, one has $J_{V_0}/A = 447$, 381, and 343 MeV fm^3 for ^{12}C, ^{40}Ca, and ^{120}Sn, respectively. One might be tempted to ascribe this behavior to the second term contained in

the brackets of the expression

$$J_{V_0}/A \approx \frac{4\pi}{3} |U_0| r_V^3 \left(1+\frac{\pi^2 a_V^2}{r_V^2 A^{2/3}}\right), \quad (68)$$

where U_0 denotes the depth of the OMP. We now show that this interpretation would be incorrect.

For simplicity we consider the simple LDA of Sec. V and a fixed energy, which allows us to drop the energy index. Let us first adopt the simple (and incorrect) assumption that the strength v_0 [Eq. (49)] of the effective interaction is density independent. Then, one has

$$V_0(r) = v_0 \rho(r), \quad J_{V_0}/A = |v_0|, \quad (69)$$

and J_{V_0}/A is thus independent of A. In other words, the dependence on mass number of the volume integral per nucleon of the isoscalar part of the OMP is due to the fact that the strength of the effective interaction depends on density. Equation (57) shows that this conclusion remains true for the improved LDA of Sec. VI.

Within our simplified assumption that the strength v_0 is independent of ρ, one has

$$U_0 = v_0 \rho_0, \quad \rho_0 = \rho_0^{(Z)} + \rho_0^{(N)}. \quad (70)$$

These relations, together with Eqs. (39) and (68) yield Eq. (69), as should be the case. They show that the depth $|U_0|$ of the real part of the isoscalar component of the OMP increases with increasing A in this simple model. This property remains true in general: In the case of the improved LDA of Sec. VI and at $E = 30$ MeV, one has $U_0 = -43.4$, -46.5, and -46.9 MeV for the depth of the isoscalar component of the OMP of the nuclei ^{12}C, ^{40}Ca, and ^{120}Sn, respectively. Hence, any argument based on Eq. (68) alone is quite dangerous.

Let us now consider the realistic case when the strength $|v_0(\rho)|$ of the effective interaction decreases with increasing density. We still restrict the discussion to the LDA of Sec. V since Eq. (57) shows that this is sufficient for our purpose. From Eqs. (39), (68), and (70), we have

$$J_{V_0}/A = |v_0(\rho_0)| \frac{r_V^3}{r_\rho^3} \left(1+\frac{\pi^2 a_V^2}{r_V^2 A^{2/3}}\right)\left(1+\frac{\pi^2 a_\rho^2}{r_\rho^2 A^{2/3}}\right)^{-1} \quad (71a)$$

$$\approx |v_0(\rho_0)| \left(\frac{r_V}{r_\rho}\right)^3 \left[1+\frac{\pi^2}{A^{2/3}}\left(\frac{a_V^2}{r_V^2}-\frac{a_\rho^2}{r_\rho^2}\right)\right]. \quad (71b)$$

It can easily be checked from Eqs. (55) and (56) that the product of the last two factors on the right-hand side of Eq. (71b) is independent of A whenever the potential V_0 is obtained by folding the density ρ with a density-independent effective interaction with a short range; this is in keeping with our considerations in the preceding paragraph. However, Fig. 1 shows that in reality v_0 depends on the density. This has two consequences: (i) The first factor on the right-hand side of Eq. (71b), i.e., the strength $|v_0(\rho_0)|$ of the effective interaction, decreases by approximately 20% between $A = 12$ and $A = 40$, because of the increase of the central density ρ_0 [Eq. (39)]; it then remains constant between $A = 40$ and $A = 208$. (ii) The product of the second and third factors on the right-hand side of Eq. (71b) smoothly decreases by about 20% between $A = 12$ and $A = 208$.

In conclusion, the rapid and then slower decrease of J_{V_0}/A with increasing A is mainly due to the density dependence of the strength of the effective interaction. The plateau observed for $A > 50$ in the curve which represents J_{V_p}/A in Fig. 18 is due to the increasing importance of the isovector and Coulomb components. It does not appear in the case of J_{V_n}/A (Fig. 19).

C. Dependence of J_W/A on mass number

The calculated (LDA) Coulomb and isovector contributions to the volume integral per nucleon of the imaginary part of the proton OMP, i.e., the quantities

$$J_{W_p}/A = -A^{-1} \int W_p(r,E)\, d^3r, \quad (72)$$

$$J_{W_C}/A = -A^{-1} \int W_C(r,E)\, d^3r, \quad (73)$$

$$J_{W_1}/A = -\alpha A^{-1} \int W_1(r, E-V_C)\, d^3r \quad (74)$$

are represented in Fig. 20, for $E = 35$ MeV. The convention is the same as in Fig. 18; the dashed curves show the values of J_{W_p}/A and of J_{W_1}/A found empirically by Becchetti and Greenlees.[28] These

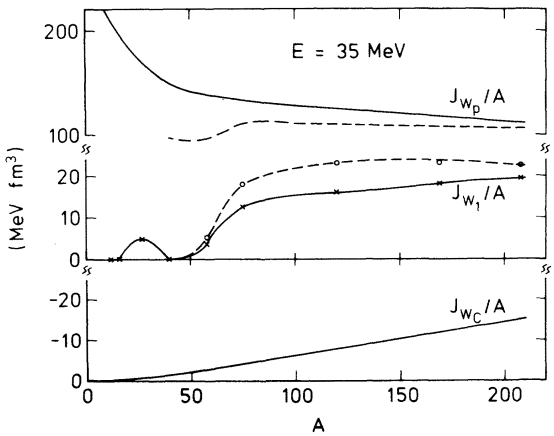

FIG. 20. Same as Fig. 18, for the imaginary part of the OMP.

authors did not introduce explicitly a Coulomb correction. The latter has been recently considered by Patterson, Doering, and Galonsky[33] who did not, however, separate it out from the value of the total W_p, which they write in the form $W_0(E - V_C) + W_1(E - V_C)$.

The interpretation of the dependence on mass number of the volume integral per nucleon of the imaginary part of the OMP is similar to that given in Sec. VII B in the case of the real part. We only note a few differences. (i) The contributions J_{W_C} and J_{W_1} of the Coulomb and of the isovector components of the OMP, respectively, approximately cancel each other in the case of low energy protons. (ii) The "strength" $w_0 = |W_0|/\rho$ of the imaginary part of the effective interaction is practically independent of ρ for $E > 120$ MeV (see Fig. 2). Together with point (i), this has the consequence that J_{W_p}/A is independent of A for $E = 140$ MeV (Fig. 17).

D. Neutron-rich skin

We now turn to the effect of assuming the existence of a neutron-rich skin at the nuclear surface. Recent α-particle scattering data indicate that the root mean square radius of the neutron distribution exceeds that of the proton distribution by $\Delta r = 0.30 \pm 0.07$ fm for ^{208}Pb.[34] This is slightly larger than theoretical estimates by Myers,[25] who also predicts that this difference smoothly decreases with decreasing A. Accordingly, we compute the proton OMP of ^{120}Sn and ^{208}Pb for a typical difference $\Delta r = 0.23$ fm between the root mean square radii of the neutron and proton distributions, in the framework of the improved LDA of Sec. VI. The results are represented by short dashes in Figs. 8, 9, 15, and 16. We see that a neutron-rich skin leads to a sizable increase of $\langle R_V^2 \rangle$ in medium-weight and heavy nuclei, and helps improving the agreement between the theoretical and empirical results.

VIII. CONCLUSIONS

The content of the present paper is threefold.

(a) We present in Sec. IV a compilation of the empirical values of the volume integrals per nucleon and of the root mean square radii of the real and of the imaginary parts of the proton OMP for the nuclei ^{12}C, ^{16}O, ^{27}Al, ^{40}Ca, ^{58}Ni, ^{120}Sn, and ^{208}Pb. Our results show that these quantities have a smooth dependence on energy and on mass number, thus encouraging their theoretical investigation from a nuclear matter approach.

(b) We parametrize in Sec. III the isoscalar, isovector, and Coulomb components of the complex OMP in uniform nuclear matter. These algebraic expressions can be used by the reader to construct the OMP in a finite nucleus from a suitable version of the local density approximation (LDA).

(c) We use two approximation schemes to obtain the OMP in a finite nucleus. The first one (Sec. V) does not introduce any adjustable parameter. It yields satisfactory values for the volume integrals per nucleon of the real and of the imaginary parts of the OMP, but too small root mean square radii. We argue in Sec. VI that the latter discrepancy was to be expected because the LDA does not retain the full influence of the range of the effective nucleon-nucleon potential when the density is not uniform. In Sec. VII, we correct for this drawback in a semiphenomenological manner by introducing an adjustable range parameter. With a reasonable value for the latter, we reach fair agreement with the empirical data.

APPENDIX

In Sec. VI, we indicated that there exists no theoretical reason for preferring the improved LDA (51b) over the form

$$\overline{V}_E(r) = (b\sqrt{\pi})^{-3} \frac{V_E(r)}{\rho(r)} \times \int \rho(r') \exp\left(-\frac{|\vec{r} - \vec{r}'|^2}{b^2}\right) d^3r' . \qquad \text{(A1)}$$

It can easily be seen that $|\overline{V}_E(0)| \geq |\tilde{V}_E(0)|$ for $b = t$; the equality is fulfilled for $b \to 0$. In Figs. 7 and 14, the short dashes correspond to the value of (A1) [and of $\overline{W}_E(r)$, constructed in the same way], for $b = 1$ fm.

A more satisfactory approach to the calculation of the real part of the OMP of a finite nucleus would consist in constructing a finite range effective interaction from the nuclear matter results, as has been done for instance by Negele.[19] In the present case, however, this effective interaction would not only be density dependent but also energy dependent. Carrying out this approach exceeds the scope of this paper. Nevertheless, a few semiquantitative considerations can be made.

Seyler and Blanchard[14,15] and later on Myers and Swiatecki[23] introduced in Thomas-Fermi calculations an energy-dependent and real effective interaction which changes sign at approximately 82 MeV. The value of this "critical" energy essentially derived from saturation requirements. Its smallness is probably associated with the fact that the Seyler-Blanchard interaction is independent of density; the corresponding mean potential field as calculated in the Thomas-Fermi approximation, changes sign at 60 MeV,[23] which is unreasonably low as compared to empirical evidence.

It is now well established that the effective in-

teraction is density dependent. Myers[25] used the phenomenological form

$$v_\rho(r) \propto e^{-(r/t)^2}(1 - d\rho^{2/3}) , \tag{A2}$$

with $d = 2$ fm^2, $t = 1.39$ fm. The short dashes in Fig. 1 represent the expression

$$F(E)(1 - d\rho^{2/3}) , \tag{A3}$$

with $d = 2.03$ fm^2 and $F(E) = (903 - 7.67E + 0.022E^2)$ MeV (10 MeV$< E <$ 140 MeV). We recall that in Sec. VI we multiplied (A3) by a Gaussian form factor with $t = 1.2$ fm. Hence, Myers's parametrization is qualitatively valid in our case.

According to Bethe,[13] the density dependence of the effective interaction is mainly due to the short-range part of the nucleon-nucleon interaction. If this would be strictly so, we should associate a finite range t only to the density independent part of the effective interaction V_0/ρ (see also Ref. 35). Hence, we also used the following improved LDA for the isoscalar component of the real part of the OMP [see Eq. (25)]

$$\mathcal{V}_0(r, E) = \sum_{i=2}^{3} \sum_{j=1}^{3} a_{ij}[\rho(r)]^i E^{j-1} + \sum_{j=1}^{3} a_{1j} E^{j-1} \times \int \rho(r') \exp\left(-\frac{|\vec{r} - \vec{r}'|^2}{t^2}\right) d^3r' . \tag{A4}$$

It can easily be seen that $\mathcal{V}_0$ and V_0 have the same volume integral in the case of a leptodermous density distribution.[24,25] We used the alternative (A4) of the LDA for the real part of the OMP, and analogously for the imaginary part. The resulting agreement with the empirical values is very similar to that found in Sec. VI. However, this approach has the drawback that the radial dependence of the second term on the right-hand side of Eq. (A4) is sufficiently different from that of the first term to introduce a small plateau in the radial dependence of $\mathcal{V}_0(r)$ at the potential surface. Moreover, the specific parametrization (25) (for instance) is somewhat arbitrary. Different powers could be used for the density ρ and for the energy E, then leading to different values for that contribution to (25) which is linear in the density.

Finally, we note that Sinha and Duggan[36] suggested to improve the LDA of Sec. V by modifying Eq. (1) which relates k_F and ρ. It appears doubtful that this procedure is justified, since this modified relation (which, incidentally, is misquoted in Ref. 36) is mainly based on corrections to the Thomas-Fermi expression for the kinetic energy; it is thus not connected with the dynamical origin of the absorptive part of the OMP.

[1]P. E. Hodgson, in *Congrès International de Physique Nucléaire*, edited by P. Gugenberger (CNRS, Paris, 1964), p. 309.

[2]J.-P. Jeukenne, A. Lejeune, and C. Mahaux, in *Proceedings of the International Conference on the Interactions of Neutrons with Nuclei, Lowell*, edited by E. Sheldon (National Technical Information Service, Springfield, 1976), Vol. 1, p. 451.

[3]G. W. Greenlees, G. J. Pyle, and Y. C. Tang, Phys. Rev. 171, 1115 (1968).

[4]D. C. Agrawal and P. C. Sood, Phys. Rev. C 11, 1854 (1975).

[5]P. E. Hodgson, Phys. Lett. B65, 331 (1976).

[6]J. Hüfner and C. Mahaux, Ann. Phys. (N.Y.) 73, 525 (1972).

[7]J.-P. Jeukenne, A. Lejeune, and C. Mahaux, Phys. Rep. C 25, 83 (1976).

[8]J.-P. Jeukenne, A. Lejeune, and C. Mahaux, Phys. Rev. C 15, 10 (1977).

[9]J.-P. Jeukenne, A. Lejeune, and C. Mahaux, in *Nuclear Self-Consistent Fields*, proceedings of the International Conference held at the International Center for Theoretical Physics, Trieste, 1975, edited by G. Ripka and M. Porneuf (North-Holland, Amsterdam, 1975), p. 155.

[10]J.-P. Jeukenne, A. Lejeune, and C. Mahaux, Nukleonika 20, 181 (1975).

[11]R. V. Reid, Ann. Phys. (N.Y.) 50, 411 (1968).

[12]K. A. Brueckner, J.-R. Buchler, S. Jarna, and R. J. Lombard, Phys. Rev. 171, 1188 (1968).

[13]H. A. Bethe, Phys. Rev. 167, 879 (1968).

[14]R. G. Seyler and C. H. Blanchard, Phys. Rev. 124, 227 (1961).

[15]R. G. Seyler and C. H. Blanchard, Phys. Rev. 131, 355 (1963).

[16]P. Haensel, Nucl. Phys. A245, 29 (1975).

[17]F. G. Perey, in *Nuclear Spectroscopy and Reactions*, edited by J. Cerny (Academic, New York, 1974), pt. B, p. 137.

[18]C. M. Perey and F. G. Perey, At. Data Nucl. Data Tables 17, 1 (1976).

[19]J. W. Negele, Phys. Rev. C 1, 1260 (1970).

[20]C. Dover and N. Van Giai, Nucl. Phys. A190, 373 (1972).

[21]N. Vinh Mau and A. Bouyssy, Nucl. Phys. A257, 189 (1976).

[22]W. T. H. Van Oers and J. M. Cameron, Phys. Rev. 184, 1061 (1969).

[23]W. D. Myers and W. J. Swiatecki, Ann. Phys. (N.Y.) 55, 395 (1969).

[24]G. Süssmann, Z. Physik A 274, 145 (1975).

[25]W. D. Myers, Nucl. Phys. A204, 465 (1973).

[26]V. Gillet and J. M. Normand, Nucl. Phys. A176, 225 (1971).

[27]J. Cugnon, Nucl. Phys. A208, 333 (1973).

[28]F. D. Becchetti and G. W. Greenlees, Phys. Rev. 182, 1190 (1969).

[29]J. Rapaport, J. D. Carlson, D. Bainum, T. Cheema, and R. W. Finlay, in *Proceedings of the International Conference on the Interactions of Neutrons with Nu-*

clei, Lowell, edited by E. Sheldon (see Ref. 2), p. 1320 (see also p. 490).
[30]B. Holmqvist, Ark. Fys. 38, 403 (1968).
[31]B. Holmqvist and T. Wiedling, Nucl. Phys. A188, 24 (1972).
[32]J. C. Ferrer, J. D. Carlson, and J. Rapaport, Nucl. Phys. A275, 325 (1977).
[33]D. M. Patterson, R. R. Doering, and A. Galonsky, Nucl. Phys. A263, 261 (1976).
[34]H. J. Gils and H. Rebel, Phys. Rev. C 13, 2159 (1976).
[35]R. Y. Cusson, H. P. Trivedi, H. W. Meldner, M. S. Weiss, and R. E. Wright, Phys. Rev. C 14, 1615 (1976).
[36]B. Sinha and F. Duggan, Phys. Lett. B47, 389 (1973).
[37]O. Karban, P. D. Greaves, V. Hnizdo, I. Lowe, N. Berovic, H. Wojciechowski, and G. W. Greenlees, Nucl. Phys. A132, 548 (1969).